Tropical Cloud Heating Profiles: Analysis from KWAJEX

COURTNEY SCHUMACHER

Department of Atmospheric Sciences, Texas A&M University, College Station, Texas

PAUL E. CIESIELSKI

Department of Atmospheric Science, Colorado State University, Fort Collins, Colorado

MINGHUA H. ZHANG

Institute for Terrestrial and Planetary Atmospheres, Marine Sciences Research Center, Stony Brook University, Stony Brook, New York

(Manuscript received 5 June 2007, in final form 13 March 2008)

ABSTRACT

Diabatic heating (or Q_1) profiles associated with specific cloud types are produced by matching synoptic cloud observations with a sounding budget analysis during the Tropical Rainfall Measuring Mission (TRMM) Kwajalein Experiment (KWAJEX), which took place in the Marshall Islands from late July through mid-September 1999. Fair-weather cumulus clouds produce up to 1 K day^{-1} of heating below 850 hPa and are associated with cooling throughout much of the rest of the troposphere. Cumulus congestus clouds produce heating on the order of 1 K day^{-1} up to 575 hPa and cooling in the mid- to upper troposphere. Cumulonimbus clouds produce heating through the depth of the troposphere, with a maximum of 3.7 K day^{-1} near 550 hPa. Cloud types indicating widespread rain (stratus or cumulus fractus of bad weather at low levels and nimbostratus at midlevels) have the largest and most elevated heating, with values $>$10 K day^{-1} above 600 hPa. Other mid- and high-level cloud types are shown to be consistent with area-averaged rain rates and Q_1 profiles. Profiles of the divergence and apparent moisture sink (or Q_2) for convective clouds are also analyzed and are shown to be consistent with the physics of the heating profiles just described.

1. Introduction

The diabatic heating associated with tropical cloud systems is often considered a driver of large-scale circulations in the tropics and extratropics (e.g., Hartmann et al. 1984). Budget studies allow the computation of bulk heating profiles associated with the ensemble of tropical convection over large regions, typically a sounding network covering an area $>$100 000 km^2 (e.g., Reed and Recker 1971). However, it is much more difficult to observe the heating profile associated with a particular cloud type.

This work is an extension of Schumacher et al. (2007), who focused on characterizing the diabatic heating from the Tropical Rainfall Measuring Mission (TRMM) Kwajalein Experiment (KWAJEX) and two other TRMM field campaigns using sounding budget analyses. However, in Schumacher et al. (2007) the role of particular cloud types in diabatic heating variations remained speculative. This study attempts to isolate the heating associated with different tropical clouds, with emphasis on fair-weather cumulus, cumulus congestus, and cumulonimbus types, by matching visual cloud observations with a sounding budget analysis over the west Pacific intertropical convergence zone (ITCZ) during KWAJEX.

2. Data and methods

KWAJEX took place in the Marshall Islands (7°–10°N, 166°–169°E; Fig. 1) from 24 July to 15 September 1999 with the purpose of studying convective processes over the tropical ocean and how these processes relate

Corresponding author address: Courtney Schumacher, Department of Atmospheric Sciences, Texas A&M University, 3150 TAMU, College Station, TX 77843-3150.
E-mail: courtney@ariel.met.tamu.edu

DOI: 10.1175/2008MWR2275.1

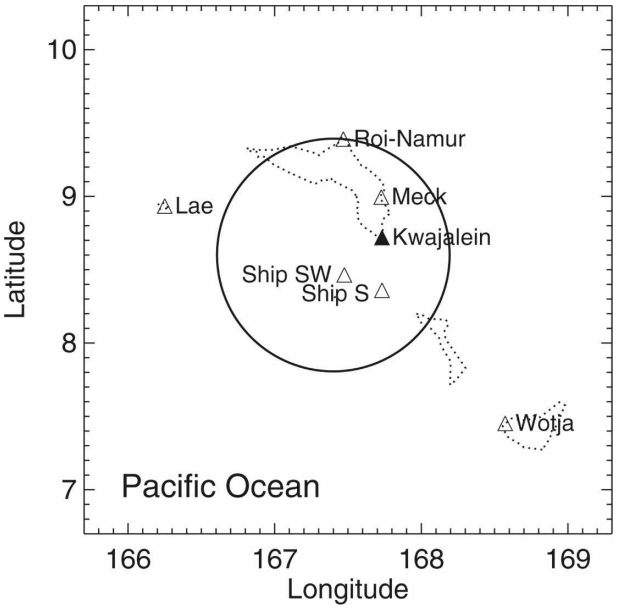

FIG. 1. The variational analysis domain (thick circle) for KWAJEX. Sounding sites are indicated by triangles. The radar and cloud observations were located at Kwajalein Island (filled triangle). Dotted lines indicate the outlines of atolls (i.e., coral islands enclosing a lagoon); the rest of the region is open ocean.

to National Aeronautic and Space Administration (NASA) TRMM satellite retrievals (Yuter et al. 2005). Kwajalein and the surrounding atolls are composed of very small islands with negligible land surface, such that the region can be considered open ocean. Further, while Kwajalein represents only one location in the ITCZ, we postulate that the diabatic heating associated with specified cloud types will be qualitatively similar in other oceanic locations.

During the field campaign, cloud observations were made by KWAJEX scientists 3 times daily [2000, 0100, and 0600 UTC (0800, 1300, and 1800 LT, respectively)] from the operations center on Kwajalein Island (filled triangle in Fig. 1). Clouds were classified according to the World Meteorological Organization's (WMO's) synoptic code (WMO 1974) into 10 types (including no cloud) at each of the following height levels: low (cloud bases >800 hPa; C_L), middle (cloud bases 800–400 hPa; C_M), and high (cloud bases <400 hPa; C_H). Cloud bases were determined by visual estimation. The KWAJEX observers also followed the WMO's basis of priorities, which assigns a priority to each cloud type; only the highest priority cloud is reported at each level regardless of the area covered.[1] Therefore, lower-priority clouds are possibly underestimated using this system. Cloud-type descriptions and WMO priorities are listed in Tables 1–3; a value of 1 represents the highest priority. While subjectivity by human observers inherently limits the accuracy of cloud classifications, temporal averaging is used in this study to minimize potential misclassifications (see also section 3). In addition, digital photo panoramas for KWAJEX were archived (available online at http://www.atmos.washington.edu/kwajex/ops-web/cloud_photos).

This study links cloud occurrence to area-averaged rainfall and diabatic heating (or the apparent heat source Q_1) profiles during KWAJEX. Rainfall is based on ground radar precipitation maps processed by the University of Washington (Houze et al. 2004). Yanai et al. (1973) defined Q_1 as

$$Q_1 = \frac{\partial \bar{s}}{\partial t} + \overline{\nabla \cdot (s\mathbf{V})} + \frac{\partial(\bar{s}\,\bar{\omega})}{\partial p}, \qquad (1)$$

where s is the dry static energy, which is equal to the sum of enthalpy and potential energy (or $s = c_pT + gz$). Overbars represent the average over the budget area. The variational analysis approach of Zhang and Lin (1997), which constrains the sounding data to

[1] During KWAJEX, only total cloud cover (octa) was recorded, not the area covered by each cloud type.

TABLE 1. KWAJEX cloud types with low-level bases.

C_L	Description	Priority	No. of observations	Frequency (%)	Rain rate (mm day^{-1})
0	No clouds with bases below 800 hPa	7	2	1.3	
1	Fair-weather cumulus (Cu)	6	33	21.6	0.8
2	Cumulus congestus (TCu)	5	47	30.7	3.1
3	Cumulonimbus (Cb) with ill-defined top	2	28	18.3	8.6
4	Stratocumulus (Sc) from spreading of Cu	3	0	0	
5	Sc not from spreading of Cu	6	1	0.7	
6	Stratus (St) not of bad weather	6	0	0	
7	St fractus or Cu fractus of bad weather	6	10	6.5	28.3
8	Cu under Sc	4	0	0	
9	Cb with cirriform top	1	32	20.9	7.3

TABLE 2. KWAJEX cloud types with midlevel bases.

C_M	Description	Priority	No. of observations	Frequency (%)	Rain rate (mm day^{-1})
0	No clouds with bases between 800 and 400 hPa	11	36	23.5	2.0
1	Semitransparent altostratus (As)	1	10	6.5	2.6
2	Thick As or nimbostratus (Ns)	2	15	9.8	17.1
3	Semitransparent altocumulus (Ac), one level	10	8	5.2	2.3
4	Semitransparent Ac, one or more levels, variable	8	8	5.2	4.3
5	Ac invading the sky as it thickens	7	3	2.0	
6	Ac from spreading of Cu, TCu, or Cb	6	9	5.9	7.4
7	Opaque Ac, two or more layers or with As or Ns	5, 9, 10	26	17.0	8.7
8	Ac with turrets	4	16	10.5	6.2
9	Ac of a chaotic sky	3	22	14.4	6.5

satisfy column-integrated budgets of mass, energy, and moisture, was used to derive the Q_1 profiles. The radar-derived rainfall was one of the analysis constraints. Rain rates and Q_1 values over the variational analysis domain were computed for 6-h periods centered on 0000, 0600, 1200, and 1800 UTC. Further details on the KWAJEX variational analysis and Q_1 structures classified by the diurnal cycle, easterly wave location, and rain thresholds can be found in Schumacher et al. (2007).

The location of the radar and sounding sites and the variational analysis domain for KWAJEX are shown in Fig. 1. Kwajalein Island is east of the center of the variational analysis domain, which has a radius of about 85 km. This radius makes the KWAJEX variational analysis area small (24 341 km^2) compared to other studies [cf. ~80 000 km^2 over the B-scale network in the Global Atmospheric Research Program (GARP) Atlantic Tropical Experiment (GATE; Thompson et al. 1979), ~217 000 km^2 in Reed and Recker's (1971) west Pacific analysis, and ~225 000 km^2 over the intensive flux array in Tropical Ocean and Global Atmosphere Coupled Ocean–Atmosphere Response Experiment (TOGA COARE; Lin and Johnson 1996)]. Because measurement errors averaged over a small domain are typically larger than those averaged over a large domain, the uncertainties of the heating profiles for KWAJEX should be large compared to other studies. In addition, sampling errors for KWAJEX should be large compared to other studies, because the sampling errors decrease with averaging scale (Mapes et al. 2003). However, a smaller budget area should be more conducive to analyzing heating profiles of individual cloud types. In addition, visibility was generally very good during KWAJEX such that cloud observations of mid- and high-level clouds and tall cumulus towers were possible though much of the region. Even on days with large particle haze, visibility was still in the tens of kilometers (A. Rangno 2007, personal communication; see also Rangno and Hobbs 2005). Finally, it is assumed that the cloud field does not vary significantly over the domain at each observation time because the region is effectively open ocean and would not be expected to show large spatial variability in forcing. Thus, the cloud observations from Kwajalein Island are considered to be generally representative of the variational analysis domain.

TABLE 3. KWAJEX cloud types with high-level bases.

C_H	Description	Priority	No. of observations	Frequency (%)	Rain rate (mm day^{-1})
0	No clouds with bases above 400 hPa	8	10	6.5	2.0
1	Cirrus (Ci) filaments not invading the sky	7	17	11.1	1.7
2	Dense Ci patches or Ci with turrets	7	8	5.2	2.2
3	Dense Ci anvil remnants	6	13	8.5	4.7
4	Ci filaments invading the sky	5	3	2.0	
5	Ci and cirrostratus (Cs) or Cs alone invading the sky, <45° above horizon	4	15	9.8	5.8
6	Ci and Cs or Cs alone invading the sky, >45° above horizon	4	22	14.4	6.8
7	Cs covering celestial dome	2	9	5.9	5.1
8	Cs not invading sky and not covering entire dome	3	23	15.0	7.0
9	Cirrocumulus (Cc) predominant	1	20	13.1	3.2
/	Upper levels obscured by lower clouds	/	13	8.5	23.3

3. Results and discussion

a. Cloud-type occurrence

Cloud observations began the afternoon of 25 July and ended the evening of 14 September. A total of 153 daytime cloud observations will be used in the following analysis. Tables 1–3 list the number of observations and frequency of occurrence of each cloud type with bases at low, mid-, and high levels, respectively. Figure 2 shows photographs taken during KWAJEX of fair-weather cumulus, cumulus congestus, and cumulonimbus clouds, which were the most commonly observed cloud-type bases during the experiment.

Table 1 shows that negligible counts of C_L 0, 4, 5, 6, and 8 were observed during KWAJEX; that is, there was rarely an absence of clouds with low-level bases (C_L 0), and stratus (St) and stratocumulus (Sc) (C_L 4–6 and 8) were seldom reported, although stratus (and/or cumulus) fractus of bad weather (C_L 7) accounted for 7% of the observations. Cumulonimbus (Cb; C_L 3 and 9) was observed 39% of the time followed by cumulus congestus (TCu; C_L 2), which accounted for 31% of the observations, and fair-weather cumulus (Cu; C_L 1), which accounted for 22% of the observations. Note that Cb, TCu, and Cu may coexist with one another, but that the synoptic code gives priority to more developed low-level clouds. This synoptic prioritization presents a limitation to the current study, so the reader should be aware of the possibility of lower-priority clouds contributing to the heating profiles of higher-priority clouds. The KWAJEX low-cloud distributions are generally consistent with the June–August (JJA) cloud climatology in Norris (1998), although Norris's climatology showed slightly lower occurrences of Cb and Cu in the Kwajalein region. The predominance of Cu, TCu, and Cb during KWAJEX is also consistent with the TOGA COARE observations from Johnson et al. (1999) of a trimodal convective cloud distribution over the tropical ocean.

Table 2 shows that no midlevel clouds (C_M 0) were observed about a quarter of the time. Altostratus (As; C_M 1 and 2) was relatively rare, with an occurrence of 7% for semitransparent clouds and 10% for thicker clouds or nimbostratus (Ns). These two cloud types have the highest priority for midlevel clouds. Altocumulus (Ac; C_M 3–9) was observed 60% of the time.

Table 3 shows that no high clouds (C_H 0) were seen 7% of the time during KWAJEX, while upper levels were obscured (C_H/) 9% of the time. Cirrocumulus (Cc; C_H 9) occurred in 13% of the observations and cirrostratus (Cs) not invading the sky (C_H 7 and 8) was observed 20% of the time. These three designations have the highest priority for high-level clouds. Cirrus (Ci) or Cs invading the sky (C_H 4–6) accounted for about a quarter of the observations, while other Ci types (C_H 1–3) were present in the other quarter of the high-cloud observations.

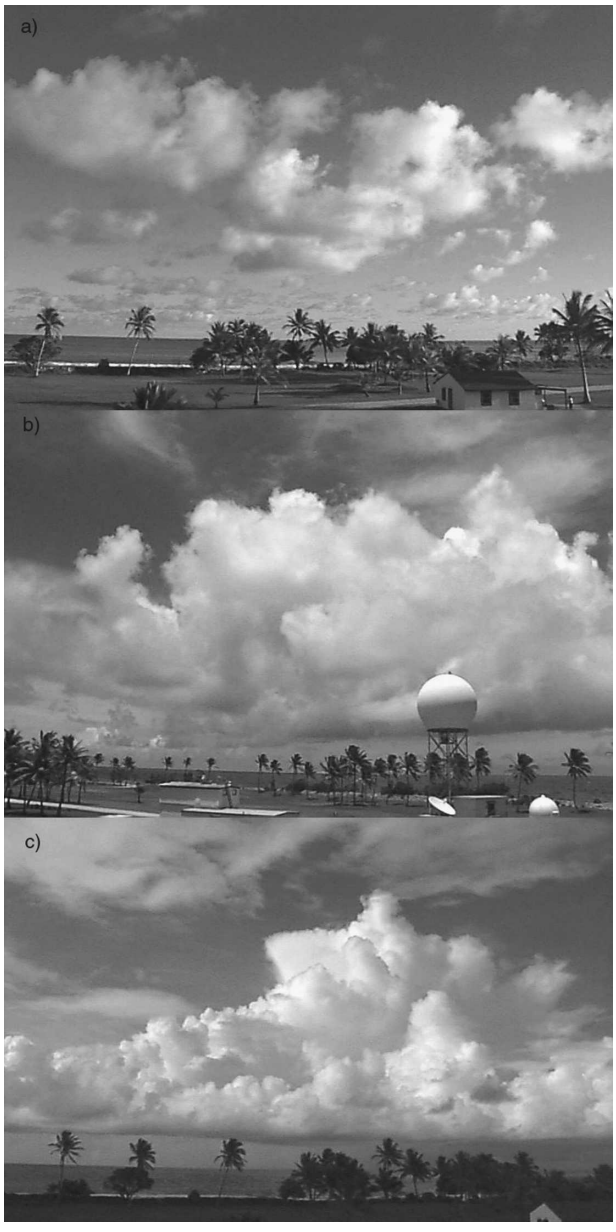

FIG. 2. Photographs of cloud types with low-level bases taken from the KWAJEX operations center: (a) fair-weather cumulus (0600 UTC 21 Aug), (b) cumulus congestus (0100 UTC 4 Aug), and (c) cumulonimbus (2000 UTC 14 Sep). (Images courtesy of the University of Washington.)

b. Cloud-type rain rates

Tables 1–3 also show the average rain rate observed by the Kwajalein radar over the variational analysis

domain during the 6-h period encompassing each cloud observation (e.g., 2100–0300 UTC rain rates for 0100 UTC cloud observations). Rain rates were not calculated for cloud types with less than eight counts (i.e., <5% of the observations).

The rain rates in Table 1 appear consistent with the low-level cloud-type designations. For example, when Cu (C_L 1) was the only evident low-level cloud, the rain rate was low (0.8 mm day^{-1}). As the clouds grew in vertical extent from TCu (C_L 2) to Cb (C_L 3 and 9), the rain rate increased from 3.1 to 8.0 mm day^{-1}. Based on aircraft observations during KWAJEX, Rangno and Hobbs (2005) showed that cumulus clouds began to precipitate once they reached 1.5 km in depth (i.e., the depth that Cu begins transitioning to TCu) and that the collision–coalescence process was especially robust in congestus clouds, which is consistent with the higher TCu rain rate. When St or Cu fractus of bad weather (C_L 7) was present, the rain rate was 28.3 mm day^{-1}, which is consistent with significant rain production by tropical convective systems that cover extensive areas.

Midlevel cloud types also show a coherent link to rain production (Table 2). Lower rain rates (<5 mm day^{-1}) occurred when midlevel clouds were absent (C_M 0) or when the midlevel clouds were semitransparent As or Ac (C_M 1, 3, and 4). Moderate rain rates (6–9 mm day^{-1}) occurred when thicker Ac (C_M 6–9) was present. The highest rain rate (17.1 mm day^{-1}) occurred when thick As or Ns (C_M 2) was observed.

At upper levels (Table 3), lower rain rates (<5 mm day^{-1}) occurred either when no ice clouds (C_H 0) were visible or in the presence of Ci (C_H 1–3) or Cc (C_H 9). Moderate rain rates (5–7 mm day^{-1}) occurred when Cs (C_H 5–8) was observed. The highest rain rate (23.3 mm day^{-1}) occurred when the upper levels were obscured (C_H/) most commonly by Ns (C_M 2) or multilayer Ac (C_M 7).

c. *Cloud-type Q_1*

The average Q_1 profile during KWAJEX is shown in Fig. 3. The main heating maximum is 1.8 K day^{-1} at 550 hPa, with a secondary heating maximum of 1.5 K day^{-1} at 750 hPa (see also Schumacher et al. 2007). The daytime Q_1 profile (i.e., the times when cloud observations were made) and the difference between the two profiles are included to show that there is a sampling bias of upper-level heating centered around 350 hPa and lower-level heating near the surface using only observations during daylight hours. This bias is likely due to the diurnal variation in shortwave heating (Mather et al. 2007), but could also be caused by variations in both cloud cover and type.

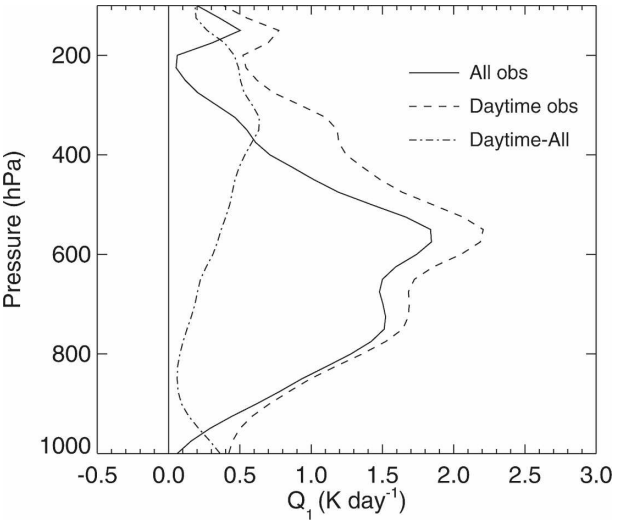

FIG. 3. KWAJEX Q_1 profiles for all observations, daytime-only (1800, 0000, and 0600 UTC) observations, and the difference between daytime and all times.

The average Q_1 profile for each cloud type is shown in Fig. 4. As with the rain-rate calculation, cloud observations were matched with the Q_1 profile computed for the 6-h period encompassing the cloud observation. It should be noted that other cloud types also contribute to each heating profile [see Warren et al. (1985) for more discussion about simultaneous cloud-type occurrence], but that the plotted profile best represents the average conditions associated with the presence of that particular cloud. In addition, Q_1 represents condensational, radiative, and vertical eddy sensible heat effects, and these effects may vary substantially from one cloud type to the next. The Q_1 profiles in Fig. 4 are broadly separated by rain rates, with low rain-rate (<5 mm day^{-1}) cloud types in the left panels, moderate rain-rate (5–9 mm day^{-1}) cloud types in the middle panels, and high rain-rate (>17 mm day^{-1}) cloud types in the right panels. Uncertainties in the Q_1 analysis are estimated to be dominated by, and similar to, those in surface precipitation (Zhang et al. 2001). Thus, stratification of the Q_1 profiles by rain rates should reduce the uncertainties in the amplitudes of the Q_1 profiles that are associated with the rain-rate bins resulting from the variational constraints. In addition, profiles are not shown for cloud types accounting for <5% of the observations (i.e., <eight counts) during the field campaign to avoid the large uncertainties related to sampling error (Mapes et al. 2003).

The Cu (C_L 1) Q_1 profile (Fig. 4a, left panel) exhibits heating below 850 hPa and cooling up to 275 hPa. The profile has a maximum heating of 1 K day^{-1} near the surface and a maximum cooling of 1.7 K day^{-1} at 450

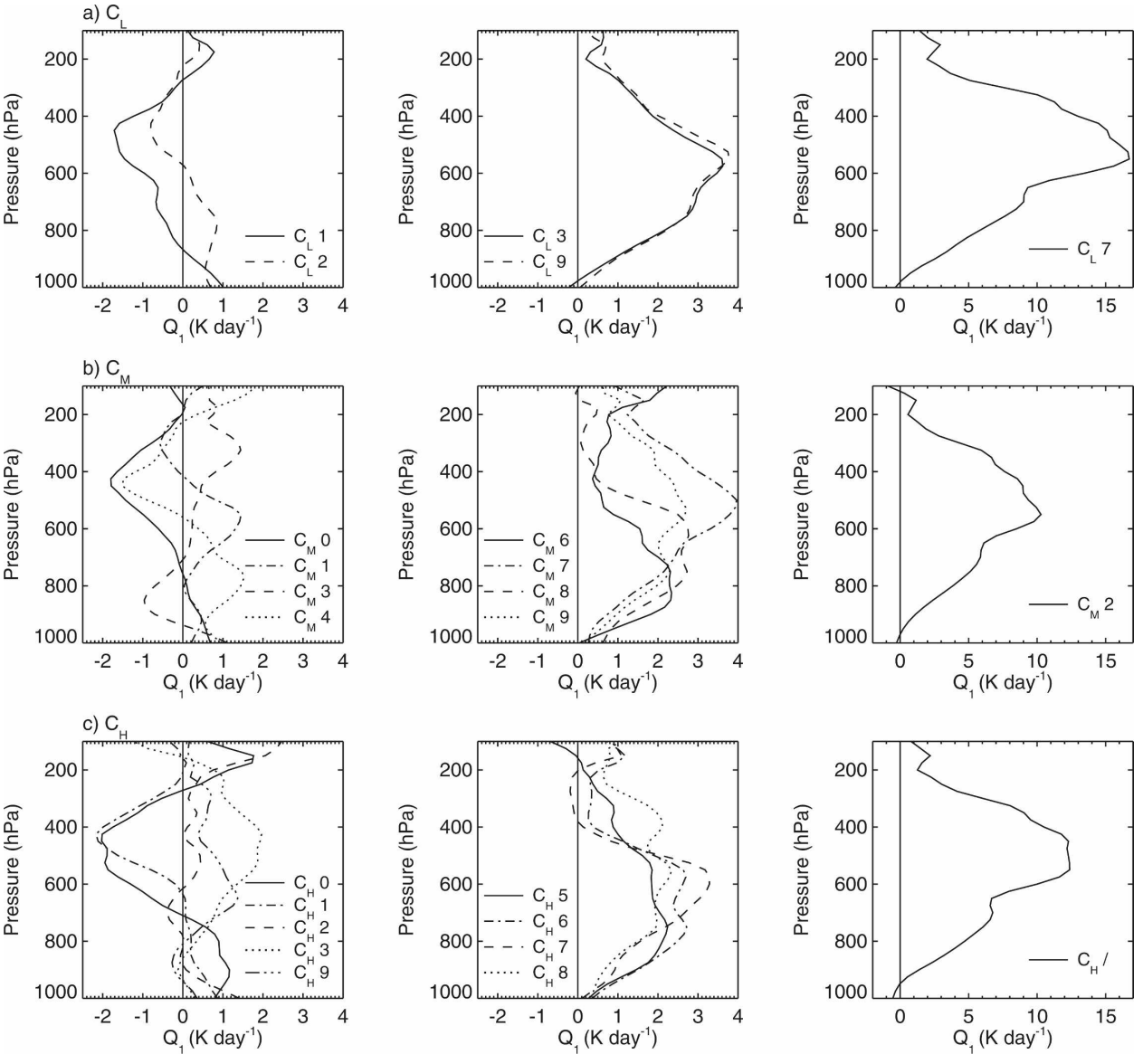

FIG. 4. Average Q_1 profiles for each cloud type during KWAJEX. (left) Low (<5 mm day^{-1}), (middle) moderate (5–9 mm day^{-1}), and (right) high (>17 mm day^{-1}) rain-rate cloud types are shown. (a) C_L: (left) Cu and TCu, (middle) Cb, and (right) St and/or Cu fractus of bad weather; (b) C_M: (left) semitransparent As and Ac, (middle) thick Ac, and (right) Ns; and (c) C_H: (left) Ci and Cc, (middle) Cs, and (right) upper levels obscured.

hPa. A secondary heating maximum occurs at 175 hPa. The lower part of this profile is similar to the undisturbed trade wind cumulus Q_1 profiles in the west Atlantic (Nitta and Esbensen 1974), except that the cooling around 800 hPa (most likely resulting from evaporation of detrained cloud material) is less pronounced in the C_L 1 profile because a strong trade wind inversion was not as prevalent during KWAJEX. The mid- to upper-level cooling near 450 hPa is likely associated with clear-sky radiative cooling, while the upper-level heating peak at 175 hPa likely reflects the radiative effects resulting from the presence of cirrus clouds and is observed in many of the cloud-type profiles in Fig. 4.

To further investigate the probable radiative effect at upper levels, Fig. 5 shows the diurnal variation of the C_L 1 Q_1 profile. Note that there was an equal occurrence of a C_L 1 at each time. Note also that the column-integrated values of the radiative component of diabatic heating Q_R during KWAJEX were -1.2, 0.3, and -0.8 K day^{-1} for 0600, 1200, and 1800 LT, respectively (Schumacher et al. 2007). In Fig. 5, the 0600 LT profile is similar to the average C_L 1 profile, but it is shifted left

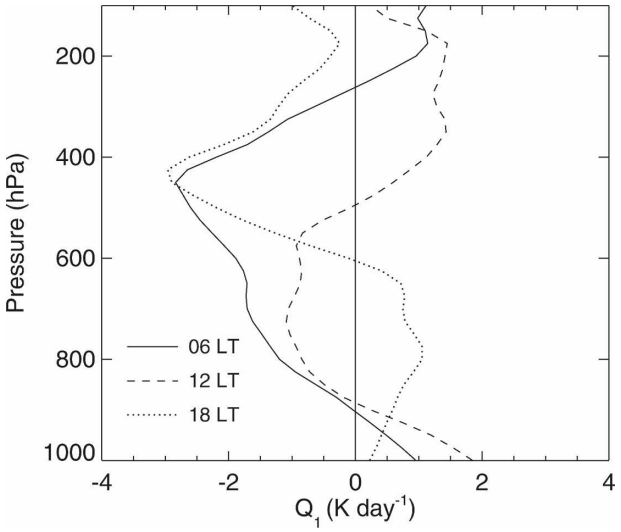

FIG. 5. Diurnal Q_1 profiles for fair-weather cumulus (C_L 1) observations during KWAJEX.

in part because Q_R is more negative in the morning than in the afternoon or early evening. The 1200 LT profile is similar to the 0600 LT profile at low levels, but the heating above 500 hPa suggests strong daytime solar absorption by the tropical atmosphere along with the high clouds commonly observed with fair-weather cumulus. The 1800 LT profile shows heating between 900 and 600 hPa, which is suggestive of more vertically developed clouds. In addition, the 1800 LT profile shows cooling at 450 hPa that is similar in magnitude to the morning. However, the 1800 LT profile shows more cooling above this level, suggesting different upper-level cloud coverage, height, and/or thickness than at 0600 LT. Figure 5 is generally consistent with the strong diurnal cycle in Q_R at upper levels observed by Mather et al. (2007) when high clouds are present over Manus Island in the west Pacific.

The TCu (C_L 2) Q_1 profile (Fig. 4a, left panel) exhibits heating on the order of 1 K day^{-1} from the surface to 575 hPa and cooling from 575 to 225 hPa, with a maximum cooling of 0.8 K day^{-1} near 450 hPa. A simple Student's t test shows that the C_L 1 and C_L 2 profiles are significantly different between 700 and 525 hPa. The deeper heating in the cumulus congestus profile indicates an enhanced latent heat release in more vertically developed clouds, while the cooling aloft is likely a mix of evaporative and radiative cooling. The diurnal variation in the C_L 2 (not shown) indicates weak upper-level cooling at 0600 LT, heating aloft at 1200 LT, and strong upper-level cooling at 1800 LT, also in general agreement with Mather et al.'s (2007) upper-level Q_R calculations in cloudy skies. Further, the average C_L 2 profile is consistent with Nitta and Esbensen's (1974) 28 June Q_1 profile, which captured disturbed trade wind conditions with clouds extending well above the trade wind inversion. The low-level heating peak around 800 hPa also coincides with the heating maximum of the initial stage in the life cycle of a tropical cloud cluster during GATE, when deep convection is minimal (Frank and McBride 1989), and of the second principal component of the TOGA COARE intensive flux array Q_1 (Tung et al. 1999). However, neither of these profiles indicated cooling aloft.

The Cb (C_L 3 and 9) Q_1 profiles (Fig. 4a, middle panel) are almost identical and exhibit heating throughout the depth of the troposphere, with maxima of ~3.7 K day^{-1} at 550 hPa. This deep heating is consistent with the large vertical extent and heavy rain rates of cumulonimbus clouds. The heating maximum in the St and/or Cu fractus of the bad weather (C_L 7) Q_1 profile (Fig. 4a, right panel) is at a similar height as in the Cb profiles, but it is almost 5 times greater in magnitude, with more heating above the peak. Half of the C_L 7 observations occur in conjunction with Ns, which is indicative of widespread convection and rain (i.e., a conglomeration of Cbs and resultant stratiform rain rather than just a handful of individual cells), and thus large Q_1 values. The C_L 7 profile is also consistent with past budget studies of large tropical convective systems (Reed and Recker 1971; Yanai et al. 1973; Frank and McBride 1989, etc.).

When no clouds with bases at midlevels are present (C_M 0), Cu and TCu are observed 90% of the time. Therefore, the C_M 0 Q_1 profile (Fig. 4b, left panel) is roughly an average of the C_L 1 and C_L 2 Q_1 profiles, with weak heating below 750 hPa and stronger cooling aloft. Semitransparent patches of Ac continually changing in appearance (C_M 4) occur three-quarters of the time with TCu, such that the C_M 4 Q_1 profile is similar to the C_L 2 Q_1 profile, but with enhanced heating between 800 and 600 hPa, which is within the height range ascribed to C_M clouds. The other semitransparent Ac cloud category (C_M 3), in which the clouds are only at one level and are unchanging in appearance, has a Q_1 profile that is somewhat opposite of the other low rain-rate cloud types, with cooling up to 1 K day^{-1} below 700 hPa, weak heating increasing from 700 to 400 hPa, and heating >1 K day^{-1} above 400 hPa (although there is a shallow heating layer near the surface associated with Cu). The heating above 400 hPa is possibly associated with the common occurrence of Cc with this cloud type. The semitransparent As (C_M 1) Q_1 profile exhibits a heating peak of 1.5 K day^{-1} at 550 hPa, the level at which these clouds roughly occur, with a secondary heating peak of 0.5 K day^{-1} at 900 hPa from Cu and TCu.

The thicker Ac (C_M 6–9) Q_1 profiles (Fig. 4b, middle panel) show heating throughout the troposphere, but with varying heights of maximum heating. Altocumulus from the spreading out of cumulus (C_M 6) has a Q_1 profile with a broad heating maximum of 2.3 K day^{-1} from 850 to 750 hPa. This cloud category occurs in conjunction with Cb 80% of the time, but the lower heating peak may indicate a preferred layer for detrainment (Zuidema 1998). Altocumulus with turrets (C_M 8) has an even broader heating maximum of 2.7 K day^{-1} from 750 to 550 hPa. Altocumulus in multiple layers or in the presence of Ns (C_M 7) has the most elevated heating of 4 K day^{-1} at 500 hPa. The Q_1 profile representing the Ac of a chaotic sky (C_M 9) is a blend of the other three Ac profiles in the middle panel. Dense As or Ns (C_M 2) has a Q_1 profile (Fig. 4b, right panel) with maximum heating of 10 K day^{-1} at 550 hPa, 2.5–4 times greater than other midlevel cloud types.

Similar to the absence of midlevel clouds, the absence of clouds with bases at high levels often occurs when Cu or TCu are present (i.e., 70% of the time) such that the C_H 0 Q_1 profile (Fig. 4c, left panel) is an average of the C_L 1 and C_L 2 Q_1 profiles. A similar argument can be made for when Ci filaments (C_H 1) predominate such that this cloud type does not appear to have a large impact on Q_1. The presence of Ci patches or cumuliform tufts (C_H 2) is associated with little vertical structure in Q_1, while the presence of dense anvil remnants of Cb (C_H 3) is linked to sizeable heating (up to 2 K day^{-1}) above 600 hPa, possibly indicating significant cloud radiative forcing at upper levels. When Cc predominates (C_H 9), the maximum heating is lower (around 650 hPa) and weaker (1.3 K day^{-1}), likely because Cc occurs 25% of the time with turreted Ac (C_M 8), which also has maximum heating around that height. However, there is a secondary heating maximum near 300 hPa.

Cirrostratus designations (C_H 5–8) indicate variations in the cover and progression of cirrostratus across the sky. The associated Q_1 profiles (Fig. 4c, middle panel) show heating on the order of 2–3 K day^{-1} through much of the lower and midtroposphere, which suggests that Cs is associated with vertical variations in Q_1 via the low- and midlevel clouds with which it occurs. Cirrostratus invading the sky (C_H 5 and 6) has more low-level heating, perhaps being associated with developing convection, while Cs not invading the sky (C_H 7 and 8) has more elevated heating associated with more mature convection. Each Cs designation shows a secondary Q_1 peak between 400 and 300 hPa, except for C_H 7. The lack of an upper-level C_H 7 heating peak is likely because this cloud type was most commonly observed at 1800 LT, when Q_R is negative. C_H 8, which has the strongest upper-level Q_1 peak, was observed much more often at 1200 LT, a time when shortwave radiative heating dominates. When upper levels are obscured (C_H/), the Q_1 profile (Fig. 4c, right panel) resembles the C_L 7 and C_M 2 profiles of strong, deep heating.

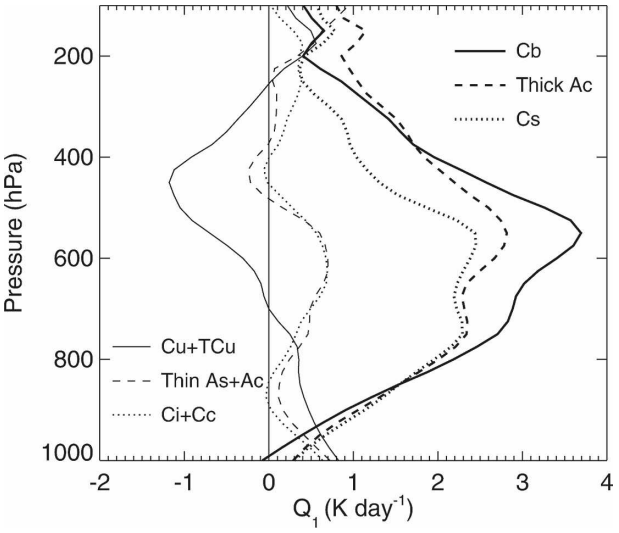

FIG. 6. Average KWAJEX cloud-type Q_1 profiles grouped by category.

Figure 6 synthesizes Fig. 4 by averaging Q_1 profiles for similar cloud types in the left and middle panels. As previously discussed, Cu and TCu (C_L 1 and 2) are associated with relatively weak heating at low levels and slightly stronger cooling in the mid- to upper troposphere. In aggregate, semitransparent As and Ac (C_M 1, 3, and 4) are associated with heating on the order of 0.5 K day^{-1} in the middle troposphere. Both Ci and Cc (C_H 1–3 and 9) appear to have a weak heating signal above 400 hPa. The presence of Cb (C_L 3 and 9) is associated with the largest heating throughout the troposphere, although thick Ac (C_M 6–9) is also associated with strong tropospheric heating, in part because these midlevel clouds commonly occur with Cb. Cirrostratus (C_H 5–8) has a weak-to-moderate heating signal in the upper troposphere in addition to stronger heating below 400 hPa associated with other cloud types.

d. C_L divergence and Q_2

While this study is primarily focused on diabatic heating profiles associated with the various cloud types observed during KWAJEX, tropical cloud systems are also strongly linked to the large-scale circulation and tropical atmosphere via divergence (Mapes and Houze 1995) and moistening (e.g., Reed and Recker 1971). Figure 7 shows the horizontal divergence and apparent

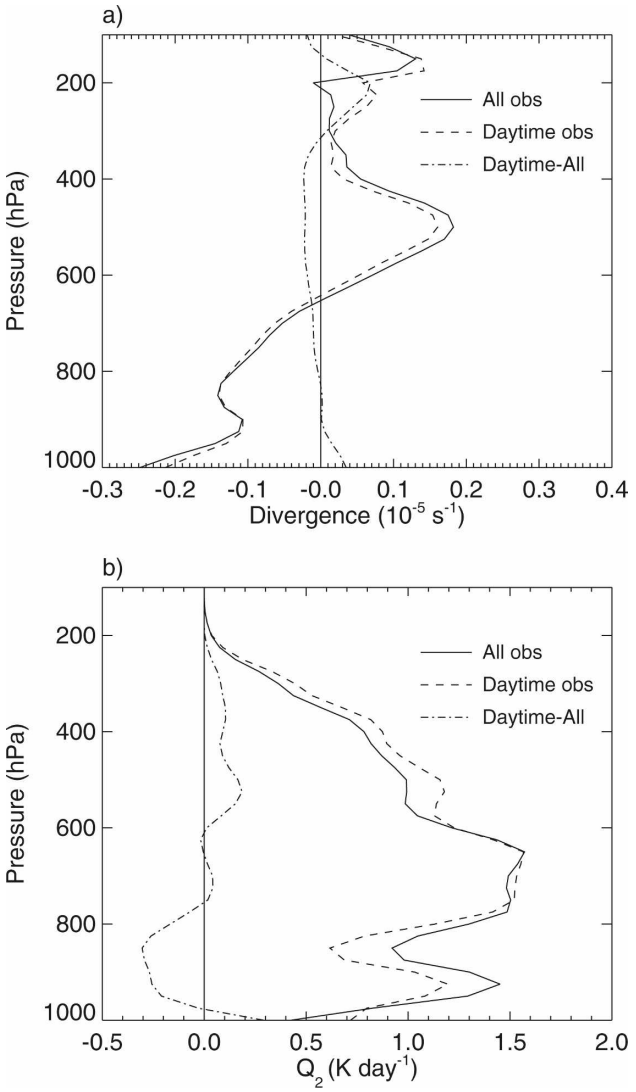

FIG. 7. KWAJEX profiles of (a) divergence and (b) Q_2 for all observations, daytime-only (1800, 0000, and 0600 UTC) observations, and the difference between daytime and all times.

moisture sink (or Q_2) profiles calculated from the variational analysis for all observations, as well as daytime-only observations, during the field campaign. Yanai et al. (1973) defined Q_2 as

$$Q_2 = -L\left(\frac{\partial \overline{q}}{\partial t} + \overline{\nabla \cdot (q\mathbf{V})} + \frac{\partial(\overline{q}\,\overline{\omega})}{\partial p}\right), \qquad (2)$$

where q is the specific humidity.

The average divergence profile in Fig. 7a indicates convergence below 650 hPa and divergence aloft with a maximum divergence value of 0.2×10^{-5} s^{-1} at 500 hPa. A secondary peak in divergence occurs at 175 hPa and a relative minimum in the low-level convergence occurs at 900 hPa. This profile suggests convective cloud populations with characteristic tops near 900, 500, and 175 hPa, similar to the horizontal divergence profile observed in the east Atlantic during GATE by Thompson et al. (1979) and consistent with Johnson et al.'s (1999) work on the trimodal distribution of oceanic convective clouds. However, the upper-level divergence peak in the KWAJEX profile is closer in height to the higher divergence peak observed in the west Pacific by Reed and Recker (1971), suggesting deeper convection than over the east Atlantic.

The average Q_2 profile in Fig. 7b indicates apparent drying (positive values) throughout the troposphere with magnitudes of 1–1.5 K day^{-1} (similar to the Q_1 magnitudes in Fig. 3) below 625 hPa and decreasing apparent drying aloft. There is also a relative minimum of drying at 850 hPa. This profile is generally consistent with the average Q_2 profiles observed during GATE (Thompson et al. 1979) and TOGA COARE (Lin and Johnson 1996); however, there is significant variation in the heights and relative magnitudes of the drying peaks between the field campaigns.

As in Fig. 3, the daytime profiles (i.e., the times when cloud observations were made) and the difference between daytime and all observations for divergence and Q_2 are included in Fig. 7 to investigate any sampling biases. In Fig. 7a, there is a tendency for weaker convergence at the surface and weaker divergence from 900 to 300 hPa during daylight hours, but the differences appear to be negligible. In Fig. 7b, there is more apparent moistening (negative values) below 775 hPa and slightly more apparent drying through the rest of the troposphere in the daytime observations. The daytime bias in Q_2 is slightly larger at low-levels compared to Q_1 (Fig. 3), possibly because of stronger vertical eddy transports of moisture near the surface. However, the daytime bias in Q_1 is much more significant at upper levels where shortwave heating effects predominate.

Figure 8 shows divergence and Q_2 profiles for C_L cloud types observed during KWAJEX. The Cu (C_L 1) divergence profile (Fig. 8a, left panel) exhibits divergence below 450 hPa and convergence above 450 hPa, consistent with the concept that fair-weather cumulus clouds commonly occur in the presence of large-scale subsidence (Nitta and Esbensen 1974). The TCu (C_L 2) divergence profile indicates a shallow layer of strong convergence from the surface up to 900 hPa, with weaker convergence up to 800 hPa. Divergence exists between 800 and 400 hPa, with convergence again above 400 hPa. Strong low-level convergence capped by a deeper divergence layer is consistent with a population of convective clouds detraining at varying heights in the midtroposphere.

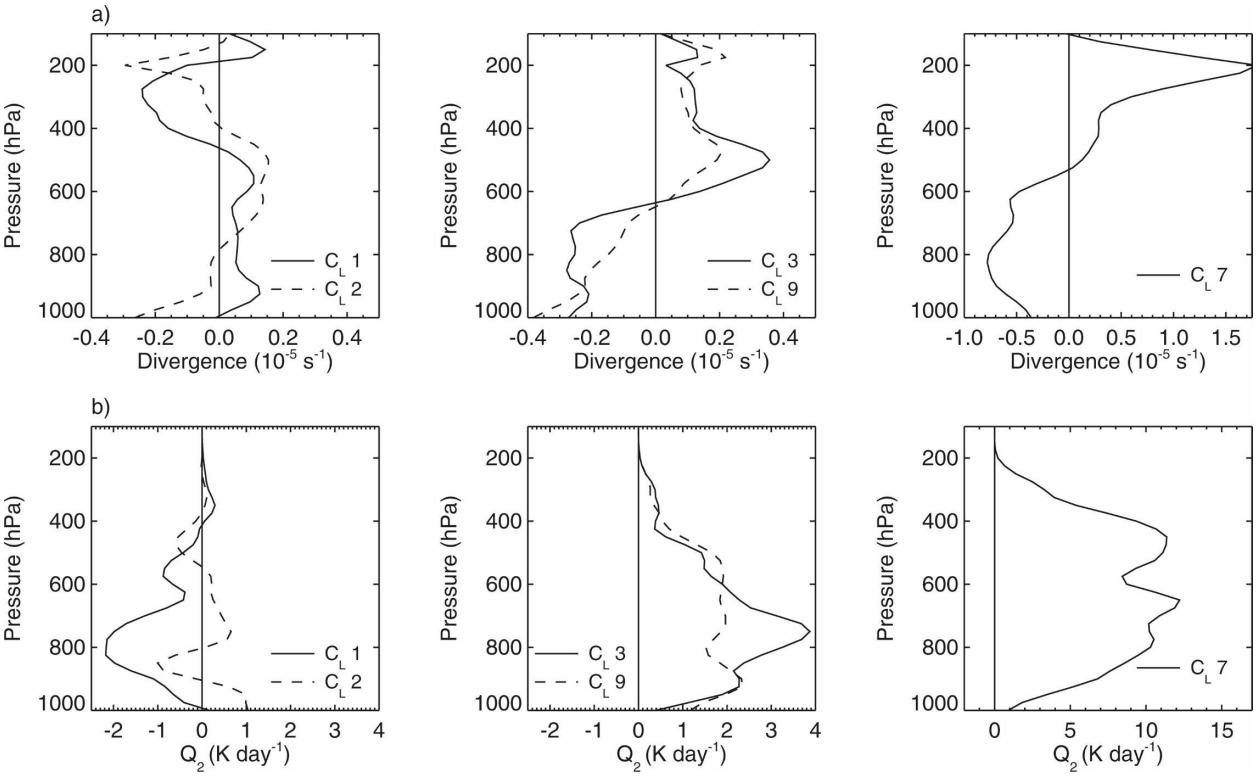

FIG. 8. Profiles of (a) divergence and (b) Q_2 for convective cloud types observed during KWAJEX.

The Cb (C_L 3 and 9) divergence profiles (Fig. 8a, middle panel) have convergence from the surface to 650 hPa and divergence throughout the rest of the mid- to upper troposphere with a peak near 500 hPa. Maximum convergence and divergence values are approximately 0.4 10^{-5} s^{-1}, which is 2–3 times the value of the less vertically developed C_L 1 and C_L 2 cloud types. While the C_L 3 and C_L 9 Q_1 profiles in Fig. 4 are almost identical, more variation is seen in the divergence profiles in Fig. 8. Cumulonimbus clouds with ill-defined tops (C_L 3) appear to have a stronger convergence–divergence couplet in the vertical than Cb with well-defined cirriform tops (C_L 9), although the difference between the profiles is only marginally statistically significant at 700 and 500 hPa. Stratus and/or Cu fractus of bad weather (C_L 7) has the strongest and deepest region of convergence with values of up to 0.8 10^{-5} s^{-1} from the surface to 525 hPa (Fig. 8a, right panel), with even stronger divergence aloft. The convergence peak near 600 hPa may be evidence of melting layer convergence in deep convective systems arising from extensive regions of stratiform rain (Mapes and Houze 1995).

The Cu (C_L 1) Q_2 profile (Fig. 8b, left panel) shows a peak in moistening at 800 hPa that can be attributed to the upward transport of moisture by shallow cumulus clouds (Nitta and Esbensen 1974). This peak is also comparable to the low-level apparent moistening observed by Johnson and Lin (1997) during convectively suppressed, light-wind periods in the equatorial west Pacific. Moistening rates are larger than heating–cooling rates for the Cu clouds, which is also consistent with the results of Nitta and Esbensen (1974). A secondary peak in moistening above 600 hPa occurs when the Cu clouds deepen at 1800 LT (as discussed in section 3c; see Fig. 5). The TCu (C_L 2) Q_2 profile also indicates two moisture source peaks—a lower peak at 850 hPa and a second peak at 475 hPa. The C_L 2 categorization does not preclude the presence of more shallow clouds, such that the C_L 2 Q_2 profile possibly represents the moistening effects of both cloud types, with the lower peak being associated with detrainment from shallow cumulus and the higher peak being associated with detrainment from cumulus congestus.

The Cb (C_L 3 and 9) Q_2 profiles (Fig. 8b, middle panel) show drying throughout the troposphere. Again, the two profiles are not as similar as in Q_1. More generally, Lin and Johnson (1996) and Johnson and Ciesielski (2000) have shown that the Q_2 profiles have more variability than the Q_1 profiles. The C_L 3 Q_2 profile has a sharp peak at 750 hPa, whereas the C_L 9 profile has a broader region of drying from 900 to 500 hPa. Cumulonimbus clouds with ill-defined tops appear

to preferentially create a larger apparent moisture sink in the lower troposphere, although the statistical significance of the difference at 750 hPa is not strong. The St and/or Cu fractus of bad weather (C_L 7) Q_2 profile (Fig. 8b, right panel) also shows drying throughout the troposphere, but is higher in magnitude with more drying aloft. The bottom heaviness in the Cb (C_L 3 and 9) Q_2 profiles and the top heaviness in the C_L 7 Q_2 profile are consistent with Johnson's (1984) postulation that the double peak of drying often observed in profiles of the apparent moisture sink in the tropics occurs from two different processes, that is, lower-level drying in convective updrafts and upper-level drying from mesoscale updrafts in stratiform rain regions. In addition, the local minimum at 600 hPa in the C_L 7 Q_2 profile may be explained by an inflection in the specific humidity profile that can be traced to the effects of melting near the 0°C level (Johnson et al. 1996).

4. Conclusions

KWAJEX cloud distributions show a predominance (i.e., at least a 50% occurrence) of low-level cumulus, midlevel altocumulus, and upper-level cirrus and cirrostratus cloud, which is consistent with the expected cloud population over an ocean ITCZ location based on published cloud climatologies (e.g., Norris 1998). Cloud types can be associated with certain ranges of rain accumulations. For example, when only Cu occurs at low levels, very low rain rates (<1 mm day^{-1}) result, whereas when Ns occurs at midlevels, very high rain rates (>15 mm day^{-1}) result. Cumulonimbus, thick Ac, and Cs cloud observations are associated with moderate (5–9 mm day^{-1}) rain rates.

Variations in cloud type with rain rate translate into variations in the vertical structure of Q_1. Small Cu clouds produce very little rain and thus do not provide much net heating to the atmosphere, but they can redistribute heat at low levels, as this study shows. Cumulus congestus provides deeper heating (up to 575 hPa), but still exhibits cooling aloft; Cb heats the depth of the troposphere, with a maximum of a few Kelvin per day near 550 hPa; and Ns provides heating at even higher heights and greater magnitudes (on the order of 10 K day^{-1}). Other mid- and high-level cloud types show enhancement of the Q_1 profile at their height of occurrence, although high-level clouds tend to have the weakest signal. The diurnal variation of cloud occurrence can also affect average Q_1 profiles. While these results seem intuitive, this study quantifies them by isolating a budget-calculated Q_1 by cloud type. This study also examines the divergence and Q_2 profiles of convective cloud types. Low-level convergence strengthens and deepens as convective clouds become more vertically and areally extensive, while the divergence near cloud top strengthens and narrows as it occurs at progressively higher heights. Both Cu and TCu tend to moisten the atmosphere, while Cb and C_L 7 (which is often associated with Ns) account for more bottom- and top-heavy drying, respectively. Explicit knowledge of heating, divergence, and moistening parsed by cloud type is a useful step in understanding how tropical convection interacts with phenomena such as tropical waves and large-scale oscillations (Mapes et al. 2006). This knowledge can also be used to improve satellite retrievals of heating profiles (Tao et al. 2006) and validate general circulation model depictions of vertical cloud structure (Williams and Tselioudis 2007).

Acknowledgments. Much appreciation to the KWAJEX Ops Center groups, whose members performed the daily cloud observations. Three anonymous reviewers provided useful comments. This research was supported by the NASA New Investigator Program and NSF Grant ATM-0449782 to Texas A&M University, NASA Grant NNG04GA22G to Colorado State University, and the DOE ARM program and NSF Climate Dynamics program to Stony Brook.

REFERENCES

Frank, W. M., and J. L. McBride, 1989: The vertical distribution of heating in AMEX and GATE cloud clusters. *J. Atmos. Sci.,* **46,** 3464–3478.

Hartmann, D. L., H. H. Hendon, and R. A. Houze Jr., 1984: Some implications of the mesoscale circulations in tropical cloud clusters for large-scale dynamics and climate. *J. Atmos. Sci.,* **41,** 113–121.

Houze, R. A., Jr., S. Brodzik, C. Schumacher, S. E. Yuter, and C. R. Williams, 2004: Uncertainties in oceanic radar rain maps at Kwajalein and implications for satellite validation. *J. Appl. Meteor.,* **43,** 1114–1132.

Johnson, R. H., 1984: Partitioning tropical heat and moisture budgets into cumulus and mesoscale components: Implications for cumulus parameterization. *Mon. Wea. Rev.,* **112,** 1590–1601.

——, and X. Lin, 1997: Episodic trade wind regimes over the western Pacific warm pool. *J. Atmos. Sci.,* **54,** 2020–2034.

——, and P. E. Ciesielski, 2000: Rainfall and radiative heating rates from TOGA COARE atmospheric budgets. *J. Atmos. Sci.,* **57,** 1497–1514.

——, ——, and K. A. Hart, 1996: Tropical inversions near the 0°C level. *J. Atmos. Sci.,* **53,** 1838–1855.

——, T. M. Rickenbach, S. A. Rutledge, P. E. Ciesielski, and W. H. Schubert, 1999: Trimodal characteristics of tropical convection. *J. Climate,* **12,** 2397–2418.

Lin, X., and R. H. Johnson, 1996: Heating, moistening and rainfall over the western Pacific during TOGA COARE. *J. Atmos. Sci.,* **53,** 3367–3383.

Mapes, B. E., and R. A. Houze Jr., 1995: Diabatic divergence profiles in western Pacific mesoscale convective systems. *J. Atmos. Sci.,* **52,** 1807–1828.

——, P. E. Ciesielski, and R. H. Johnson, 2003: Sampling errors in rawinsonde-array budgets. *J. Atmos. Sci.,* **60,** 2697–2714.

——, S. Tulich, J. Lin, and P. Zuidema, 2006: The mesoscale convection life cycle: Building block or prototype for large-scale tropical waves? *Dyn. Atmos. Oceans,* **42,** 3–29.

Mather, J. H., S. A. McFarlane, M. A. Miller, and K. L. Johnson, 2007: Cloud properties and associated radiative heating rates in the tropical western Pacific. *J. Geophys. Res.,* **112,** D05201, doi:10.1029/2006JD007555.

Nitta, T., and S. Esbensen, 1974: Heat and moisture budget analyses using BOMEX data. *Mon. Wea. Rev.,* **102,** 17–28.

Norris, J. R., 1998: Low cloud type over the ocean from surface observations. Part II: Geographical and seasonal variations. *J. Climate,* **11,** 383–403.

Rangno, A. L., and P. V. Hobbs, 2005: Microstructures and precipitation development in cumulus and small cumulonimbus clouds over the warm pool of the tropical Pacific Ocean. *Quart. J. Roy. Meteor. Soc.,* **131,** 639–673.

Reed, R. J., and E. E. Recker, 1971: Structure and properties of synoptic-scale wave disturbances in the equatorial western Pacific. *J. Atmos. Sci.,* **28,** 1117–1133.

Schumacher, C., M. H. Zhang, and P. E. Ciesielski, 2007: Heating structures of the TRMM field campaigns. *J. Atmos. Sci.,* **64,** 2593–2610.

Tao, W.-K., and Coauthors, 2006: Retrieval of latent heating from TRMM measurements. *Bull. Amer. Meteor. Soc.,* **87,** 1555–1572.

Thompson, R. M., Jr., S. W. Payne, E. E. Recker, and R. J. Reed, 1979: Structure and properties of synoptic-scale wave disturbances in the intertropical convergence zone of the eastern Atlantic. *J. Atmos. Sci.,* **36,** 53–72.

Tung, W.-W., C. Lin, B. Chen, M. Yanai, and A. Arakawa, 1999: Basic modes of cumulus heating and drying observed during TOGA-COARE IOP. *Geophys. Res. Lett.,* **26,** 3117–3120.

Warren, S. G., C. J. Hahn, and J. London, 1985: Simultaneous occurrence of different cloud types. *J. Climate Appl. Meteor.,* **24,** 658–667.

Williams, K. D., and G. Tselioudis, 2007: GCM intercomparison of global cloud regimes: Present-day evaluation and climate change response. *Climate Dyn.*, **28,** 231–250, doi:10.1007/s00382-007-0232-2.

WMO, 1974: Manual on codes. Vol. 1. WMO Publication 306, 348 pp.

Yanai, M., S. Esbensen, and J.-H. Chu, 1973: Determination of bulk properties of tropical cloud clusters from large-scale heat and moisture budgets. *J. Atmos. Sci.,* **30,** 611–627.

Yuter, S. E., R. A. Houze Jr., E. A. Smith, T. T. Wilheit, and E. Zipser, 2005: Physical characterization of tropical oceanic convection observed in KWAJEX. *J. Appl. Meteor.,* **44,** 385–415.

Zhang, M. H., and J. L. Lin, 1997: Constrained variational analysis of sounding data based on column-integrated budgets of mass, heat, moisture, and momentum: Approach and application to ARM measurements. *J. Atmos. Sci.,* **54,** 1503–1524.

——, ——, R. T. Cederwall, J. J. Yio, and S. C. Xie, 2001: Objective analysis of the ARM IOP data: Method and sensitivity. *Mon. Wea. Rev.,* **129,** 295–311.

Zuidema, P., 1998: On the 600–800-mb minimum in tropical cloudiness. *J. Atmos. Sci.,* **55,** 2220–2228.